

Tuning Charged Localized Excitons in Monolayer WSe₂ via Coupling to a Relaxor Ferroelectric

Qiaohui Zhou¹, Fei Wang¹, Ali Soleymani¹, Kenji Watanabe², Takashi Taniguchi³, Jiang Wei¹, and Xin Lu^{1*}

¹*Department of Physics and Engineering Physics, Tulane University, New Orleans, Louisiana 70118, United States*

²*Research Center for Electronic and Optical Materials, National Institute for Materials Science, 1-1 Namiki, Tsukuba 305-0044, Japan and*

³*Research Center for Materials Nanoarchitectonics, National Institute for Materials Science, 1-1 Namiki, Tsukuba 305-0044, Japan*

Abstract: The discovery of single photon emitters (SPEs) in two-dimensional (2D) layered materials has greatly inspired numerous studies towards utilizing the system for quantum science and technology. Thus, the dynamic control of SPEs, including neutral and charged emitters, is highly desirable. In addition to the electric control, strain tuning is particularly attractive for the 2D materials since it can activate SPEs which are formed upon localizing free excitons. While strain engineering has been demonstrated for free and neutral localized excitons, few were shown on charged localized excitons which require an additional gate control. In this article, we show the strain-tunable charged localized excitons by transferring a top-gated monolayer semiconductor on a relaxor ferroelectric. Importantly, we unveil an enhanced interaction between the localized oscillating dipoles and the nanodomains. We further demonstrate the strain-dependent circular polarization and tunable rates of energy shifts under a magnetic field. Our results imply that the integration of 2D materials with relaxor ferroelectrics provides a rich platform for nanophotonics and quantum photonics.

The emergent interest in lead-based relaxor ferroelectrics (RE-FEs) is largely attributed to their giant piezoelectric coefficients [1]. As one of the most well-known RE-FEs, (1-x)Pb(Mg_{0.33}Nb_{0.67})O_{3-x}(PbTiO₃) (PMN-PT) has been widely used to engineer the magnetic [2, 3]

and optical [4, 5] properties via interfacial interaction. Particularly, the integration of single photon emitters (SPEs) with PMN-PT as a piezoelectric substrate is attractive for novel quantum device applications, such as the strain-activated quantum light emitting diodes (Q-LEDs) [6–8]. SPEs in the two-dimensional (2D) layered materials are localized excitons (LXs), which are formed when free excitons are trapped by local defect or strain potentials [9]. As a result, strain has been demonstrated to be efficient in creating SPEs and modulating their energies in a monolayer WSe₂ [10, 11]. While most earlier work focused on neutral LXs with almost no discussion on the charged ones, the charged LXs are central to quantum photonics and quantum communication due to the absence of electron-hole (e-h) exchange interaction [12]. On the other hand, despite being broadly studied [13–15], the underlying mechanism on the large piezoelectric response of PMN-PT is still under debate [16]. In other words, the microscopic picture on strain-tuning of LXs on RE-FEs has not been completely understood.

Independent charge and strain controls

In this article, we study the strain-control of charged LXs by transferring a top-gated monolayer WSe₂ on the PMN-PT piezoelectric substrate. During the poling process (Methods), polar nanodomains in the PMN-PT will be rotated towards the [001] direction and result in net polarization. Applying an external electric field parallel (anti-parallel) to the poling direction will lead to expansion (contraction) in the out-of-plane direction and compressive (tensile) strain in-plane (Fig. 1a). Strain can be applied to samples attached on the PMN-PT substrate with magnitude of the transferred strain depending on the interfacial quality [5]. To introduce the inverse piezoelectric effect, an external voltage (i.e., strain voltage) needs to be applied to either the back side of the PMN-PT (V_{BS}) or a front pad (V_{TS}) close to the sample (Fig. 1b). Despite the smaller electric-field induced deformation, unintentional doping effect from the front pad is much more insignificant (Supplementary Note 1). We note that unintended doping is a common side effect in strain engineering [17–19]; therefore, we added a top gate to achieve the charge control. By tuning the top gate voltage (V_{TG}), we can compensate for the doping and extract the pure strain effect from the PMN-PT. An independent gate control also provides a platform to explore how charged excitons respond to the RE-FE, since exfoliated samples are generally neutral or slightly n-doped. Before discussing the LXs, we first characterized the strain effect from our substrate by using the free neutral exciton X^0 in WSe₂ as a sensor. Figure 1c shows the photoluminescence (PL) spectra of X^0 from an encapsulated WSe₂ (the only device with bottom hexagonal boron nitride, h-BN) at

~ 4 K. $V_{BS} = -125$ V (-50 V) corresponds to -2.5 kV/cm (-1 kV/cm) in the PMN-PT (thickness: 0.5 mm) and results in a shift of 1.9 meV (0.6 meV) to X^0 , which is comparable to an earlier study [18].

Strain-tuning of neutral localized excitons

Having demonstrated that our device configuration is capable of strain-tuning at the cryogenic temperature, we removed the bottom h-BN layer and lowered the excitation power for LXs. Figure 2a shows the tuning of neutral LXs, D1 and D2, as a function of V_{BS} from $+200$ V ($+4$ kV/cm) to 0 V. Due to the long-range e-h exchange interaction, D1 and D2 have fine structure splitting (FSS) of ~ 0.7 meV. As V_{BS} decreased, both D1 and D2 blue shift, which is consistent with the poling direction. Compared to previous results on neutral LXs in WSe₂, the magnitude of shift indicates the variation of strain is $< 0.1\%$ [10] for V_{BS} ranging from $+200$ V to -200 V (Supplementary Fig. 4 for V_{BS} from -200 V to 0 V). We plotted the energies of D1 and D2 in two sweeping directions (Fig. 2b & 2c). D1 shows negligible hysteresis, while D2 shows small shifts of $0.2 - 0.4$ meV at some voltages. Since D1 and D2 were measured simultaneously within a laser spot (~ 1 μ m), the discrepancy could not originate from the global effect of the substrate (More neutral LXs from the same measurements were shown in Supplementary Fig. 5). Instead, we hypothesize the observed hysteresis could be attributed to the local interaction between a nanodomain in the PMN-PT and the localized oscillating dipole in WSe₂. In other words, the difference originates from the low-angle polar domains [15] and the polarization axis of the neutral LXs, both of which vary depending on the location. We note that this observation has not been shown before, because most previous experiments [10, 11, 18] were performed with a layer of metal (or graphite) between the sample and the substrate. The metal layer could cause electric field screening, though strain can be transferred. This implies the interaction is a Coulomb type and depends on distance. While the neutral LXs with one electron-hole pair exhibit coupling to the substrate, the singly charged exciton, which has one extra electron/hole, should exhibit even more pronounced hysteresis.

Charged localized excitons on PMN-PT

We tune the top gate voltage (V_{TG}) to n-dope the sample. Injected electrons fill the lowest states in the conduction bands, at the K and K' valleys. Due to the spin-valley locking effect and the valley dependent optical selection rule [20], σ^+ polarized light which couples to the K valley can generate ensembles of spin up electrons in the K' valley as a result of the optical spin pumping [21]. Since the two electrons form a triplet state (Fig. 3a), the three-particle system is called the triplet trion

(X_T^-) which emits co-polarized (σ^+) light. While the long-range e-h exchange interaction, a main depolarized path for the free excitons, can flip the K valley e-h pair to the K' valley. The resulting state is the singlet trion (X_S^-) with cross-polarized (σ^-) emission (Fig. 3b). Note that the X_T^- and X_S^- states are not degenerate due to the exchange interaction (including long-range e-h, short-range e-h, and electron-electron), splitting energy (δ_{ex}) reached 7 meV in the h-BN-encapsulated sample (Supplementary Fig. 6) [22], which is consistent with the calculated value (6 meV) [23]. While δ_{ex} is proportional to the Coulomb potential $V(k)$ and thus being influenced by the dielectric environment. $V(k)$ scales with $\frac{1}{\epsilon}$ where $\epsilon = \frac{\epsilon_{top} + \epsilon_{bottom}}{2}$. The much larger ϵ from PMN-PT [24] should result in $\delta_{ex} < 0.2$ meV. However, as we do not observe smaller FSS (resulting from the long-range e-h interaction) from the neutral LXs (Fig. 2a), we still consider $\delta_{ex} \sim 7$ meV in the following discussion. The emergence of cross-polarized X_T^- (Fig. 3c) and co-polarized X_S^- (Fig. 3d) requires additional intra-/inter-valley scattering. Consequently, co-polarized X_T^- is dominant under circular excitation, particularly on resonance [21].

We apply the single particle picture as described above to the LXs. The signature of a singly charged LX is the appearance of a single peak with no splitting [25]. Different from earlier studies on localized trions where the WSe₂ device is placed on a Si/SiO₂ substrate [26, 27], the charged LX, S1 in Fig. 3e, shifts with V_{TG} . Similar shift has been studied in quantum dots and explained by the quantum-confined Stark effect (QCSE) [28, 29], but QCSE could not account for our observed redshift (Supplementary Note 2). One possible explanation is the charged LX interact with the Fermi sea, which strengthens the binding of the state and hence the energy decreases before radiative recombination [30]. Consequently, S1 peak red-shifts with an increasing number of electrons in the monolayer. We remark that while such shift is absent in earlier reports, it is common among charged LXs on the piezoelectric PMN-PT from our measurements, indicating the interaction-induced shift could be related to the details of the substrate, such as the nanodomains or the large dielectric constant of the PMN-PT [24].

Next, we extracted the degree of circular polarization (DCP: $\frac{I_{co} - I_{cross}}{I_{co} + I_{cross}}$) in Fig. 3f, and found that DCP is constant ($0.14\% \pm 0.02\%$) as a function of V_{TG} , which implies it is the interaction within the trion that dominates the depolarization. Therefore, electrons in the Fermi sea (induced by V_{TG}) have negligible effect on the polarization. Since density of the free electrons affects the energy of LXs, we apply the strain voltage from the front pad (V_{TS}) to mitigate the unintentional doping effect.

Strain-tuning of charged localized excitons

Figure 3g shows the energy of S1 as a function of V_{TS} in two sweeping directions. V_{TG} was kept at +17 V during the measurements. We first confirmed the V_{TS} -induced doping effect is negligible by comparing the V_{TS} -dependent shift to Fig. 3e. A positive V_{TS} should induce electron doping, if any, and red-shift the charged LX. Yet, S1 blue-shifts when V_{TS} changes from -150 V to +150 V, which implies the capacitance-induced doping is minor. Unlike the ferroelectric gating [31, 32], polarization from RE-FEs is much smaller and hence we do not consider the polarization-induced doping. In fact, a large polarization will prohibit the observation of neutral LXs in the broad range of -200 V to +200 V as shown in Fig. 2 and Supplementary Fig. 4, which confirms that the polarization-induced doping is suppressed in our PMN-PT substrates. The trend of energy shift in Fig. 3g is opposite to that in Fig. 2, since strain voltage is applied from the opposite side. In other words, both positive V_{TS} and negative V_{BS} cause in-plane compressive strain and result in a blueshift. Compared with the neutral LXs, energy shift from a charged LX exhibits a much larger hysteresis. Difference between the two sweeping directions reaches 2.3 meV at $V_{TS} = 0$ V, which is substantially larger than 0.4 meV at $V_{BS} = 0$ V (Fig. 2c). This observation confirms our hypothesis on the local Coulomb-type interaction between the nanodomains and LXs.

We further plotted the V_{TS} -dependent DCP in Fig. 3h. The circular polarization decreases from $\sim 10\%$ at -150 V to $\sim 0\%$ at +150 V. When $V_{TS} < 0$ V (> 0 V) and induces tensile (compressive) strain to the sample, DCP enhances (reduces) as the peak red-shifts (blue-shifts). The same trend is reproduced from another negatively charged LX, S2 (Supplementary Fig. 9). The measured polarization is given by $DCP = \frac{1}{1+2\frac{\tau_r}{\tau_s}}$ [33], where τ_r and τ_s are the radiative and spin/valley lifetimes, respectively. Our measured results indicate the ratio $\frac{\tau_r}{\tau_s}$ increases (decreases) with tensile (compressive) strain. While radiative lifetime is insensitive to a small variation of strain [18], the spin/valley lifetime should be responsible for the V_{TS} -dependent tuning. Scattering of electrons from one band to another is generally through the following three paths in WSe₂: the long-range e-h exchange interaction, the spin-flip intravalley scattering and the spin-conserved intervalley scattering. The long-range e-h exchange interaction is on the order of \sim ps, which is too fast compared to the radiative lifetime of LXs (>1 ns) [34], and therefore could not explain the change of DCP. Instead, the slower intravalley and intervalley scattering should be the main reason for strain-tuning polarization. The valley lifetime of resident electrons was found to range from 100 ps to tens of nanosecond at 10 K [35], and the variation was explained by strain mediated

electron-phonon coupling. Our observed decreased DCP under compression is also supported by first-principles calculations which show that compressive strain enhances the spin-flip coupling in the lowest conduction band [36] and consequently reduces the spin lifetime of resident electrons.

Imbalanced strain effect under a magnetic field

To better understand the V_{TS} -dependent polarization, we apply an magnetic field (B) in the Faraday geometry. Figure 4a shows the evolution of K and K' valleys under a finite B . When $B < 0$ T, bands in the K (K') valleys shift downwards (upwards) with different magnitudes, resulted from the additive effect of spin, valley and orbital angular momentum [37]. The single peak at zero B would split into two branches. Our chosen excitation is resonant with the high-energy peak (P+) for $B < 0$ T, but the low-energy peak (P-) should dominate due to thermal equilibrium, particularly when the splitting is large at high $|B|$. As a result, the intensity ratio, I_{P+}/I_{P-} , reflects the competition between optical selection and thermal equilibrium. We showed the ratio in Fig. 4b from -3 T to -6 T when the split peaks are spectrally resolved. Consistent with the V_{TS} -dependent DCP (Fig. 3g), I_{P+}/I_{P-} is the strongest when $V_{TS} = -150$ V, and it decreases gradually towards high $|B|$ when splitting increases. Same trends were also observed for $V_{TS} = 0$ V and +150 V.

We further showed the B -dependent splitting ($\Delta E = E_{co} - E_{cross}$) of S1 peak in Fig. 4c and fitted the data by $\Delta E = g\mu_B B$, where $\mu_B = 58 \mu eVT^{-1}$ is the Bohr magneton. The extracted $|g| = 4.15 \pm 0.04$ is consistent with that of the free X_T^- in an h-BN-encapsulated sample [38, 39]. However, it is uncommon to see $|g| < 5$ for LXs in WSe₂ [26, 27, 40], and the substantially smaller $|g|$ only occurs for charged LXs (Supplementary Fig. 10). We also measured the values of g -factors at $V_{TS} = -150$ V and $V_{TS} = +150$ V (Supplementary Fig. 11), and neither shows a pronounced change. This implies that the abnormal g -factor could be associated with the presence of PMN-PT, which makes our charged LXs different from those in the h-BN encapsulated samples. On the other hand, $|g|$ of ~ 4 also indicates the S1 peak is a localized bright trion in a shallow trap, and it inherits the band structure from the host monolayer.

We subsequently plotted the B -dependent energy shifts for both P+ and P- from 0 T to -6 T at $V_{TS} = -150$ V, 0 V and +150 V. For Zeeman splitting of a singly charged LX, both split peaks should shift linearly with B and the magnitudes of both slopes are $\frac{|g|}{2}$, i.e., $|k_+| = |k_-| = \frac{|g|}{2}$. Intriguingly, the rates of shift are asymmetric and changes with V_{TS} . $\frac{|k_+|}{|k_-|}$ decreases from 85.7 at -150 V to 2.3 at 0 V, and 0.7 at +150 V. Very similar trends have also been observed at $B > 0$ T

with $\frac{|k_+|}{|k_-|} = 12.9, 4.0$ and 0.9 for -150 V, 0 V and $+150$ V (Supplementary Fig. 12), suggesting the effect from circular excitation is not major [41, 42]. The different rates of shift, with $|k_+| < |k_-|$, have been observed in free trions and explained by the Landau level quantization of both initial and final states [43]. We noticed that our observed rates at $+150$ V are similar to the shifts in Ref. [43]. Meanwhile, we are also aware that diamagnetic shifts have been applied to explain the asymmetric shift for a single quantum dot when the average energy of both peaks increases quadratically with $|B|$ [25]. The diamagnetic shift is given by $\Delta E_{dia} = e^2 \langle r^2 \rangle B^2 / 8\mu$, where $\langle r^2 \rangle$ is related to the electron-hole overlap (size of the exciton) and μ is the reduced mass. In 2D transition metal dichalcogenides, a giant field is needed for the observation of diamagnetic shifts from the $1s$ state X^0 because of the small Bohr radius [44]. Nevertheless, theory predicts that the diamagnetic shifts are larger for trion due to the increasing inter-particle distance. Moreover, ΔE_{dia} even increases linearly with the dielectric constant of the surrounding environment [45]. According to the model in Ref. [45], we obtained $\Delta E_{dia} \sim 0.4$ meV at $|B| = 6$ T by taking the average dielectric constants of PMN-PT and h-BN. We plotted the average energies of P+ and P- for each V_{TS} (Supplementary Fig. 13) and found an increase of energy with $|B|$ for -150 V and 0 V. Considering the spectral diffusion of LXs, our observed shifts of average energies matches very well with the calculated $\Delta E_{dia} \sim 0.4$ meV, which also explains why $|k_+|$ is larger than $|k_-|$ for -150 V and 0 V. Interestingly, we found that $|k_+| \approx |k_-|$ with $|k_+|$ being slightly smaller at $+150$ V. Note that ΔE_{dia} is dependent on the reduced mass, which is calculated by taking the effective masses of the particles involved. Since the effective mass (m^*) of an electron is affected by the curvature of the band with $m^* = \frac{\hbar^2}{d^2E/dk^2}$, strain could also modify the curvature (e.g. flattening the band) thus changing the reduced mass. When $B \neq 0$ T, the degeneracy of K and K' valleys is lifted, which leads to one of the valleys being more modulated by the strain. As a result, the rates of shifts are unequal between the split two peaks (i.e., $|k_+| \neq |k_-|$). Despite the strain-dependent reduced mass could also affect ΔE_{dia} , the tiny $\Delta E_{dia} \sim 0.4$ meV at $|B| = 6$ T, together with spectral diffusion, makes it hard to distinguish the difference between -150 V and 0 V. Yet, the rates of shift, $\frac{|k_+|}{|k_-|}$ is more sensitive.

Conclusions

To summarize, our work demonstrates an enhanced interaction between the charged localized excitons in a monolayer WSe₂ and the nanodomains in a piezoelectric substrate. We attributed the enhanced interaction to the presence of an additional charge compared to the neutral excitons.

As a result, the charged localized exciton exhibits a larger hysteresis in energy between the two sweeping direction of strain controls. To the best of our knowledge, for the first time we showed the gate-dependent, interaction-induced energy shifts from a localized exciton. We explained the tunable circular polarization by strain-mediated spin/valley lifetime of the resident electrons. In addition, we further observed the tunable energy shifts under a magnetic field and controlled the rates of shifts by varying the strain voltage. We remark that the negatively charged dark exciton (D^-), with both electrons at the lowest conduction bands, is very likely to have even stronger interaction with the relaxor ferroelectric. We also note that our applied electric field is small compared to the field required to rotate the polarization axis of the charge neutral GaAs quantum dots [46]. Further measurements with larger electric fields and magnetic fields will provide more insight into the integration of monolayer semiconductors with relaxor ferroelectrics, and pave way for potential applications in nanophotonics and quantum photonics.

Methods

Device fabrication

Electron beam lithography was used to deposit 5 nm Ti/100 nm Au metal contacts on both sides of the PMN-PT substrate. Before the sample-transfer process, the PMN-PT substrate was poled at room temperature by applying a direct current (DC) electric field to the backside. After reaching the targeted poling voltage (-300 V) in 5 minutes, we held the electric field for 30 minutes and released the field back to 0 V in 5 minutes [47]. Mechanically exfoliated WSe₂ (2D Semiconductors), few-layer graphene/graphite and hexagonal boron nitride (h-BN) were transferred on top of a PMN-PT piezoelectric substrate by a polydimethylsiloxane-based dry-transfer method [48]. The stacked device is illustrated in Fig 1b.

Optical measurements

Low-temperature magneto-optical measurements were performed in a closed-cycle cryostat (AttoDry 1000, Attocube Systems) equipped with a superconducting magnet. The samples were cooled to ~ 3.7 K and positioned by a piezoelectric nanopositioners (Attocube Systems). Both the 633-nm and 730-nm continuous-wave excitation lasers were collimated and focused onto the sample through an objective (NA = 0.81, Attocube Systems), with a spot diameter around 1 μm . The PL emission was collected by the same objective and directed to a high-resolution spectrometer (HRS-750, Teledyne Princeton Instruments), in which it was dispersed by a 1200 g/mm grating. A charged-coupled device (PYL-400BRX, Teledyne Princeton Instruments) was used as the detector.

For polarization-resolved measurements, a $\lambda/4$ waveplate was placed after the beam-splitter, and a $\lambda/2$ waveplate, followed by a fixed-polarization analyzer, was placed before the spectrometer. Strain and top-gate voltages were applied through Keithley 6487 and Keithley 2400 source meters, respectively.

-
- [1] S.-E. Park and T. R. ShROUT, *J. Appl. Phys.* **82**, 1804 (1997).
 - [2] C. Thiele, K. Dörr, O. Bilani, J. Rödel, and L. Schultz, *Phys. Rev. B* **75**, 054408 (2007).
 - [3] T. Nan, Z. Zhou, M. Liu, X. Yang, Y. Gao, B. A. Assaf, H. Lin, S. Velu, X. Wang, H. Luo, et al., *Sci. Rep.* **4**, 3688 (2014).
 - [4] R. Trotta, P. Atkinson, J. Plumhof, E. Zallo, R. O. Rezaev, S. Kumar, S. Baunack, J. Schröter, A. Rastelli, and O. G. Schmidt, *Adv. Mater.* **24**, 2668 (2012).
 - [5] J. Martín-Sánchez, R. Trotta, A. Mariscal, R. Serna, G. Piredda, S. Stroj, J. Edlinger, C. Schimpf, J. Aberl, T. Lettner, et al., *Semicond. Sci. Technol.* **33**, 013001 (2018).
 - [6] A. Branny, S. Kumar, R. Proux, and B. D. Gerardot, *Nat. Commun.* **8**, 15053 (2017).
 - [7] C. Palacios-Berraquero, D. M. Kara, A. R.-P. Montblanch, M. Barbone, P. Latawiec, D. Yoon, A. K. Ott, M. Loncar, A. C. Ferrari, and M. Atatüre, *Nat. Commun.* **8**, 15093 (2017).
 - [8] C. Palacios-Berraquero, M. Barbone, D. M. Kara, X. Chen, I. Goykhman, D. Yoon, A. K. Ott, J. Beitzner, T. Taniguchi, K. Watanabe, et al., *Nat. Commun.* **7**, 12978 (2016).
 - [9] M. Toth and I. Aharonovich, *Annu. Rev. Phys. Chem.* **70**, 123 (2019).
 - [10] O. Iff, D. Tedeschi, J. Martín-Sánchez, M. Moczala-Dusanowska, S. Tongay, K. Yumigeta, J. Taboada-Gutiérrez, M. Savaresi, A. Rastelli, P. Alonso-González, et al., *Nano Lett.* **19**, 6931 (2019).
 - [11] C. Chakraborty, A. Mukherjee, H. Moon, K. Konthasinghe, L. Qiu, W. Hou, T. Peña, C. Watson, S. M. Wu, D. Englund, et al., *Optica* **7**, 580 (2020).
 - [12] M. Atatüre, D. Englund, N. Vamivakas, S.-Y. Lee, and J. Wrachtrup, *Nat. Rev. Mater.* **3**, 38 (2018).
 - [13] H. Takenaka, I. Grinberg, S. Liu, and A. M. Rappe, *Nature* **546**, 391 (2017).
 - [14] M. Eremenko, V. Krayzman, A. Bosak, H. Playford, K. Chapman, J. Woicik, B. Ravel, and I. Levin, *Nat. Commun.* **10**, 2728 (2019).
 - [15] A. Kumar, J. N. Baker, P. C. Bowes, M. J. Cabral, S. Zhang, E. C. Dickey, D. L. Irving, and J. M. LeBeau, *Nat. Mater.* **20**, 62 (2021).
 - [16] T. Rojac, *Commun. Mater.* **4**, 12 (2023).
 - [17] P. Hernández López, S. Heeg, C. Schattauer, S. Kovalchuk, A. Kumar, D. J. Bock, J. N. Kirchoff, B. Höfer, K. Greben, D. Yagodkin, et al., *Nat. Commun.* **13**, 7691 (2022).
 - [18] Z. An, P. Soubelet, Y. Zhumagulov, M. Zopf, A. Delhomme, C. Qian, P. E. Faria Junior, J. Fabian,

- X. Cao, J. Yang, et al., *Phys. Rev. B* **108**, L041404 (2023).
- [19] A. Kumar, D. Yagodkin, R. Rosati, D. J. Bock, C. Schattauer, S. Tobisch, J. Hagel, B. Höfer, J. N. Kirchhof, P. H. López, et al., arXiv preprint arXiv:2312.07332 (2023).
- [20] D. Xiao, G.-B. Liu, W. Feng, X. Xu, and W. Yao, *Phys. Rev. Lett.* **108**, 196802 (2012).
- [21] C. Robert, S. Park, F. Cadiz, L. Lombez, L. Ren, H. Tornatzky, A. Rowe, D. Paget, F. Sirotti, M. Yang, et al., *Nat. Commun.* **12**, 5455 (2021).
- [22] M. He, P. Rivera, D. Van Tuan, N. P. Wilson, M. Yang, T. Taniguchi, K. Watanabe, J. Yan, D. G. Mandrus, H. Yu, et al., *Nat. Commun.* **11**, 618 (2020).
- [23] H. Yu, G.-B. Liu, P. Gong, X. Xu, and W. Yao, *Nat. Commun.* **5**, 3876 (2014).
- [24] M. Thiercelin, H. Dammak, and M. P. Thi, in *2010 IEEE International Symposium on the Applications of Ferroelectrics (ISAF)* (IEEE, 2010), pp. 1–4.
- [25] M. Bayer, G. Ortner, O. Stern, A. Kuther, A. Gorbunov, A. Forchel, P. Hawrylak, S. Fafard, K. Hinzer, T. Reinecke, et al., *Phys. Rev. B* **65**, 195315 (2002).
- [26] X. Lu, X. Chen, S. Dubey, Q. Yao, W. Li, X. Wang, Q. Xiong, and A. Srivastava, *Nat. Nanotechnol.* **14**, 426 (2019).
- [27] M. Brotons-Gisbert, A. Branny, S. Kumar, R. Picard, R. Proux, M. Gray, K. S. Burch, K. Watanabe, T. Taniguchi, and B. D. Gerardot, *Nat. Nanotechnol.* **14**, 442 (2019).
- [28] G. Wen, J. Lin, H. Jiang, and Z. Chen, *Phys. Rev. B* **52**, 5913 (1995).
- [29] P. Tamarat, T. Gaebel, J. Rabeau, M. Khan, A. Greentree, H. Wilson, L. Hollenberg, S. Praver, P. Hemmer, F. Jelezko, et al., *Phys. Rev. Lett.* **97**, 083002 (2006).
- [30] D. Van Tuan, S.-F. Shi, X. Xu, S. A. Crooker, and H. Dery, *Phys. Rev. Lett.* **129**, 076801 (2022).
- [31] Y. Zhang, W. Jie, P. Chen, W. Liu, and J. Hao, *Adv. Mater.* **30**, 1707007 (2018).
- [32] J. Choi, K. J. Crust, L. Li, K. Lee, J. Luo, J.-P. So, K. Watanabe, T. Taniguchi, H. Y. Hwang, K. F. Mak, et al., *Nano Lett.* (2024).
- [33] G. Kioseoglou, A. Hanbicki, M. Currie, A. Friedman, D. Gunlycke, and B. Jonker, *Appl. Phys. Lett.* **101** (2012).
- [34] C. K. Dass, M. A. Khan, G. Clark, J. A. Simon, R. Gibson, S. Mou, X. Xu, M. N. Leuenberger, and J. R. Hendrickson, *Adv. Quantum Technol.* **2**, 1900022 (2019).
- [35] M. Ersfeld, F. Volmer, L. Rathmann, L. Kotewitz, M. Heithoff, M. Lohmann, B. Yang, K. Watanabe, T. Taniguchi, L. Bartels, et al., *Nano Lett.* **20**, 3147 (2020).
- [36] P. E. F. Junior, K. Zollner, T. Woźniak, M. Kurpas, M. Gmitra, and J. Fabian, *New J. Phys.* **24**, 083004 (2022).
- [37] C. Robert, H. Dery, L. Ren, D. Van Tuan, E. Courtade, M. Yang, B. Urbaszek, D. Lagarde, K. Watanabe, T. Taniguchi, et al., *Phys. Rev. Lett.* **126**, 067403 (2021).
- [38] E. Liu, J. van Baren, Z. Lu, M. M. Altairy, T. Taniguchi, K. Watanabe, D. Smirnov, and C. H. Lui,

- Phys. Rev. Lett. **123**, 027401 (2019).
- [39] Z. Li, T. Wang, Z. Lu, M. Khatoniar, Z. Lian, Y. Meng, M. Blei, T. Taniguchi, K. Watanabe, S. A. McGill, et al., Nano Lett. **19**, 6886 (2019).
- [40] A. Mukherjee, K. Shayan, L. Li, J. Shan, K. F. Mak, and A. N. Vamivakas, Nat. Commun. **11**, 5502 (2020).
- [41] W. Li, X. Lu, J. Wu, and A. Srivastava, Nat. Nanotechnol. **16**, 148 (2021).
- [42] C. Jiang, A. Rasmita, W. Xu, A. Imamoglu, Q. Xiong, and W.-B. Gao, Phys. Rev. B **98**, 241410 (2018).
- [43] T. P. Lyons, S. Dufferwiel, M. Brooks, F. Withers, T. Taniguchi, K. Watanabe, K. Novoselov, G. Burkard, and A. I. Tartakovskii, Nat. Commun. **10**, 2330 (2019).
- [44] A. V. Stier, K. M. McCreary, B. T. Jonker, J. Kono, and S. A. Crooker, Nat. Commun. **7**, 10643 (2016).
- [45] M. Van der Donck, M. Zarenia, and F. Peeters, Phys. Rev. B **97**, 195408 (2018).
- [46] J. D. Plumhof, V. Krápek, F. Ding, K. Jöns, R. Hafenbrak, P. Klenovský, A. Herklotz, K. Dörr, P. Michler, A. Rastelli, et al., Phys. Rev. B **83**, 121302 (2011).
- [47] M. Otoničar, A. Bradeško, S. Salmanov, C. Chung, J. Jones, and T. Rojac, Open Ceramics **7**, 100140 (2021).
- [48] A. Castellanos-Gomez, M. Buscema, R. Molenaar, V. Singh, L. Janssen, H. S. Van Der Zant, and G. A. Steele, 2D Mater. **1**, 011002 (2014).

Acknowledgments: X.L. and Q. Z. acknowledge support from Tulane University startup fund and the Louisiana Board of Regents Support Fund (BoRSF) under award # LEQSF(2022-25)-RD-A-23. K.W. and T.T. acknowledge support from the JSPS KAKENHI (Grant Numbers 21H05233 and 23H02052) and World Premier International Research Center Initiative (WPI), MEXT, Japan. J.W. and F.W. are grateful for the support from the National Science Foundation under Grant 1752997 and the Louisiana Board of Regents under Grant 082ENH-22. We also acknowledge the support from the Micro/Nano Fabrication Facility and Coordinated Instrument Facility of Tulane University.

Author Contributions: X.L. conceived the project. Q.Z. and X.L. carried out the optical spectroscopy measurements and wrote the paper, aided by F.W. K.W. and T.T. provided the h-BN crystals. Q.Z., F.W., and A.S. prepared the samples. X.L. and J.W. supervised the project. All authors were involved in analysis of the experimental data and contributed extensively to this work.

Competing interests: The authors declare no competing interests.

Correspondence and requests for materials should be addressed to Xin Lu (xlu5@tulane.edu).

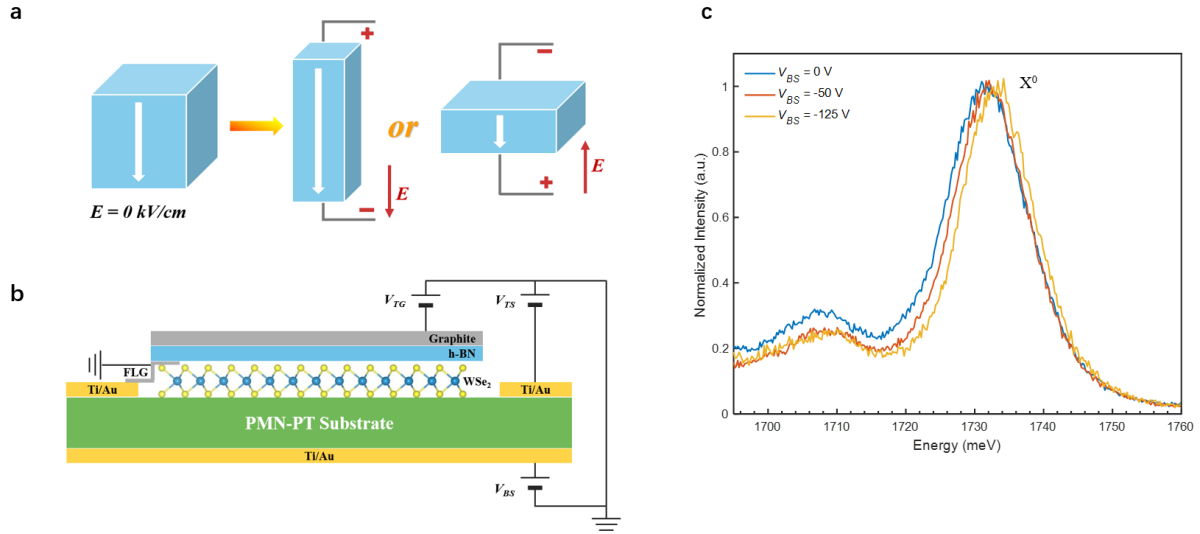


Fig. 1: Strain-tuning of monolayer WSe_2 on a PMN-PT piezoelectric substrate. **a**, Sketch of a poled PMN-PT substrate with electric field applied parallel or anti-parallel to the poling direction, which produces deformations in both the out-of-plane and in-plane directions. **b**, Schematic of the device consisting of graphite, hexagonal boron nitride (h-BN), monolayer WSe_2 flake, and few layer graphene (FLG) on the PMN-PT substrate. The graphene layer is connected to a metal electrode and functions as the grounded pad. The graphite layer works as the top gate (V_{TG}) with h-BN as the dielectric. Strain voltage can be applied from the back (V_{BS}) or through an empty metal electrode on the front (V_{TS}). **c**, PL spectra of monolayer WSe_2 under three different strain voltages (V_{BS}) at ~ 4 K. The neutral exciton X^0 red-shifts by 0.6 meV and 1.9 meV at $V_{BS} = -50$ V and -125 V, respectively. $V_{BS} = -125$ V corresponds to an effective electric field of -2.5 kV/cm to the substrate. Since a finite V_{BS} introduces doping to the monolayer sample, V_{TG} -dependent PL scan is needed for each V_{BS} to identify the charge neutral region. Excitation for **c**: 1.96 eV. Power: $10 \mu\text{W}$.

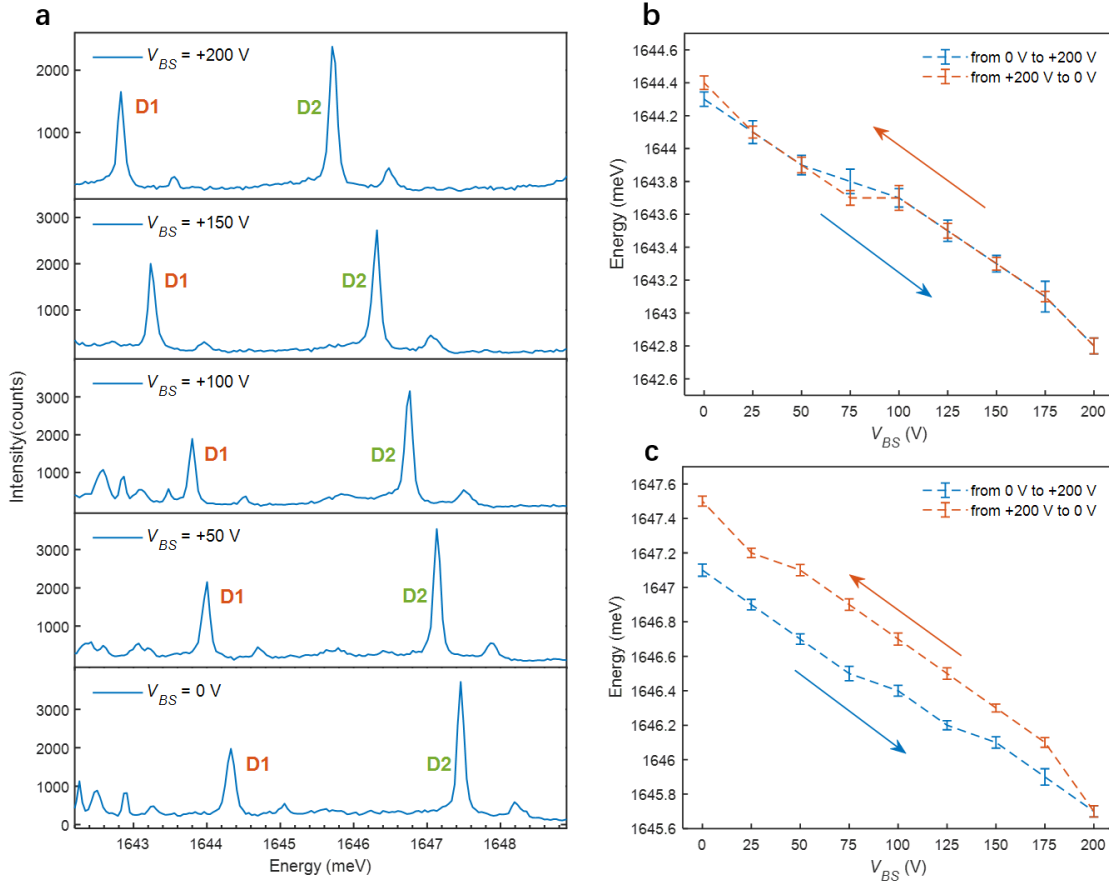


Fig. 2: Energy shifts of neutral localized excitons (LXs) as a function of back strain V_{BS} . **a**, PL spectra of neutral LXs, D1 and D2, under an applied strain voltage ranging from +200 V to 0 V on the PMN-PT substrate. **b, c**, Peak energies of D1 and D2 as a function of V_{BS} from two sweeping directions. Data from the 0 V to +200 V (+200 V to 0 V) sweep are shown in blue (red). Error bars are from the mean deviation with 60 spectra taken at each V_{BS} . Excitation: 1.70 eV. Power: 150 nW.

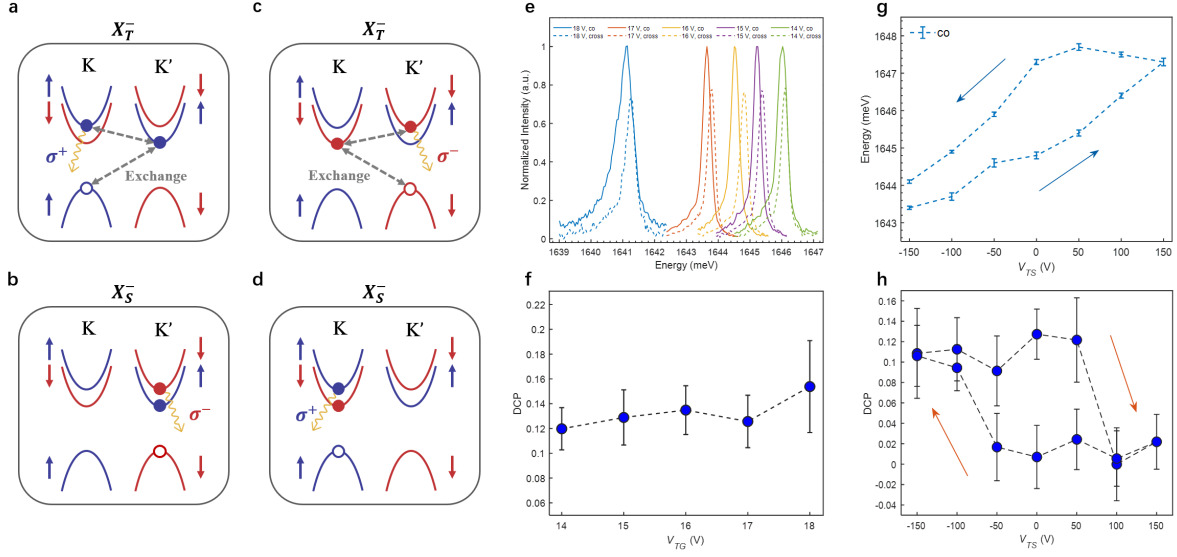


Fig. 3: Tuning a charged localized exciton (LX) by the front strain voltage (V_{TS}). a-d, Spin-valley configurations of the triplet (X_T^-) and singlet (X_S^-) trions in monolayer WSe₂. Blue (red) lines represent the spin up (down) bands in the K and K' valley. Short-range e-h and electron-electron exchange interactions are shown by the dashed lines. e, Circular polarization-resolved PL spectra of charged LX, S1, as V_{TG} changes from +14 V to +18 V. Co-polarized (Cross-polarized) spectra are shown by the solid (dashed) lines. f, Degree of circular polarization (DCP) extracted from the V_{TG} -dependent PL measurements. g, Co-polarized peak energy of S1 as a function of V_{TG} from two sweeping directions. h, DCP from two sweeping directions. Arrows in g & h indicate the tuning directions of V_{TG} . Error bars in f-h originated from the mean deviation of the peak intensities with more than 10 spectra taken for voltage. Propagation of uncertainty leads to larger error bars in f & h. Excitation for e-h: 1.96 eV. Power: 300 nW.

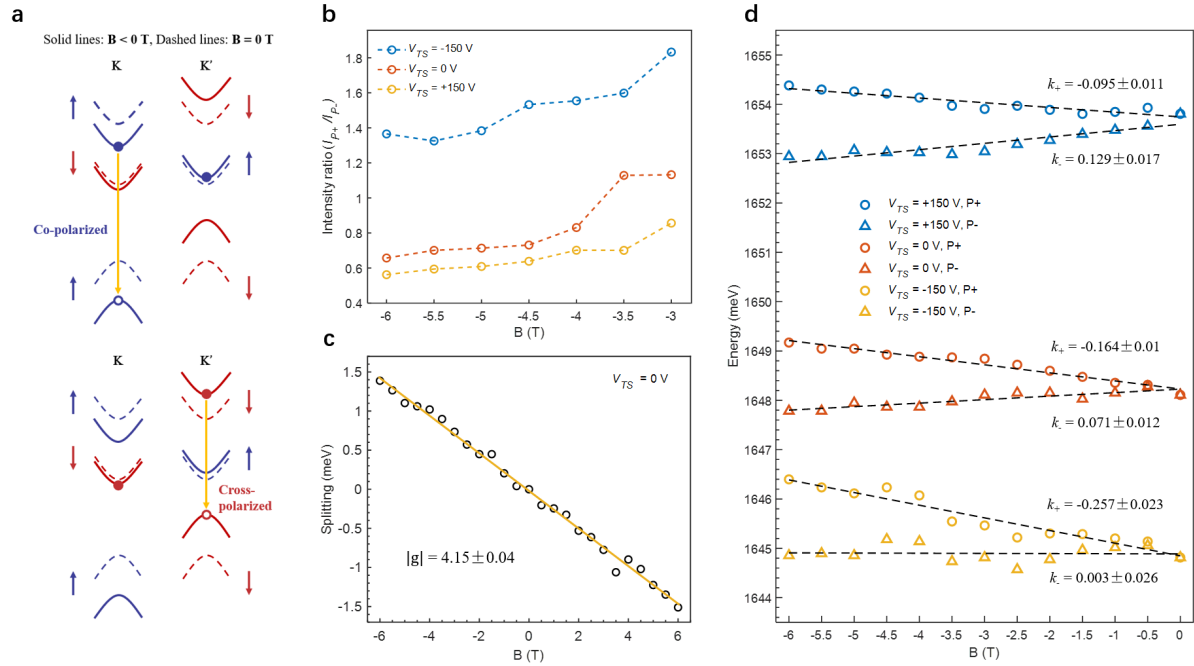


Fig. 4: Strain-tunable Zeeman splitting of the charged localized exciton (LX) S1. **a**, Schematics of energy levels in the K and K' valleys for WSe₂ when $B = 0$ T (dashed lines) and $B < 0$ T (solid lines). **b**, Magnetic field dependence of intensity ratio (I_{P+}/I_{P-}) with $V_{TS} = -150$ V, 0 V, and 150 V. **c**, Splitting energy of S1 as a function of B at $V_{TS} = 0$ V. Experimental data are shown by dots, and fitting result is displayed by the yellow line. The value of the g -factor is shown only as magnitude. **d**, Magnetic field dependence of energy shifts for peaks P+ and P- at $V_{TS} = +150$ V (blue), 0 V (red), and -150 V (yellow). Dashed lines represent the rates of shifts from fitting. Error bars arise from fit uncertainty. Excitation for **b-d**: 1.96 eV. Power: 300 nW.